Sensors and Materials, Vol. 8, No. 2 (1996) 113–136
MYU Tokyo

S & M 0229

Analytical Characterization of Piezoresistive Square-Diaphragm Silicon Microphone

Edvard Kälvesten, Lennart Löfdahl[1] and Göran Stemme

Department of Signals, Sensors and Systems, Royal Institute of Technology,
S-10044 Stockholm, Sweden
[1]Thermo and Fluid Dynamics, Chalmers University of Technology,
S-41296 Göteborg, Sweden

(Received September 30, 1994; accepted May 12, 1995)

Key words: silicon microphone, piezoresistive strain gauge, analytical characterization

An analytical energy method has been used to derive the characteristics of a square-diaphragm piezoresistive silicon microphone. All relevant mechanical and acoustical effects of the sensor characteristics are included in the method. First, the energy contributions are calculated and then identified with equivalent acoustical impedances. These equivalent impedances are used in the electrical analogy. The method is applied to a piezoresistive microphone having a square diaphragm over its cavity. A special vent channel which equalizes the static air pressure between the cavity and the ambient has been included in the model. Good agreement between the theoretical analysis and experimental data on fabricated microphones was obtained.

1. Introduction

Piezoresistive silicon microphones for applications in turbulence measurements have previously been designed, fabricated and tested.[1–3] Key features of these microphones are the piezoresistive strain gauges, the diaphragm, the air gap of the cavity and the vent channel for equalization of the static pressure. Two parameters are especially important in the design of the microphones. Firstly, for a typical boundary layer the smallest flow eddies have a length on the order of 100 μm. To resolve these small eddies the side length of the diaphragm must be of the same scale or smaller. Secondly, the pressure fluctuations of the smallest eddies are weak, on the order of a few Pa, requiring a relatively sensitive microphone. To meet these two conflicting requirements on the microphone characteristics

(a small diaphragm area generally means a low pressure sensitivity), a complete acoustical model of the microphone is required.

One method of simulating a microphone is to use analytical formulae based on equivalent electrical circuits.[4] This method, which is based on the small deflection theory in which nonlinear effects are neglected,[5] is limited by the availability of analytical expressions of the characteristic parameters, i.e., the equivalent electrical impedances of the mechanical and acoustical elements. This analogy has been applied to microphones with circular[4] as well as square diaphragms.[6] For the circular diaphragms the deflection can be handled easily, while for the square diaphragms, a flat diaphragm approximation has been used.[7] However, for piezoresistive microphones with square diaphragms, this approximation is not sufficiently accurate. One way of dealing with this problem is to use the characteristic parameters of a known circular diaphragm with an equivalent radius of $a/\sqrt{\pi}$, where a is the square-diaphragm side length.[1–3]

Another approach is to use a method based on finite-element analysis (FEA) which handles differential equations including nonlinear terms.[7] This is a powerful method which is applicable to extremely complex structures. For a structure with specific dimensions, the FEA method is also beneficial for verification of the analysis results. However, one advantage of analytical expressions is that they provide better insight into the design parameters and their influence on the desired microphone characteristics.

In this paper we characterize a silicon microphone using an analytical energy method.[8] This method makes it possible to include all relevant energy terms corresponding to the stiffness of the diaphragm to bending and tensile forces, the acoustical mass of the diaphragm and of the fluid in the front of the diaphragm, the stiffness of the air-gap cavity, and the acoustical mass as well as the frictional losses of the vent channel. To simplify the calculations, the energy and power expressions are identified with equivalent electrical impedances and an electrical analogy is employed. The results of the theoretical analysis are also compared with experimental data.

2. Sensor Design and Fabrication

A cross-sectional view of the fabricated piezoresistive microphone is shown in Fig. 1. The important features of the sensor are the small (100×100 μm) and thin (0.4 μm) diaphragm, the deep cavity (3 μm) and the narrow vent channel cross section (0.1×5 μm). For comparison, a microphone with a diaphragm side length of 300 μm is fabricated as well. Piezoresistive readout is provided by two active piezoresistors located on the diaphragm and two other passive piezoresistors which are integrated near the diaphragm, making it possible to connect the four piezoresistors in a Wheatstone bridge. In the present design, with the turn-around of the active piezoresistors located at a distance of $0.2a$ from the diaphragm edge, the dominant contribution to the resistance change is assumed to be the longitudinal strain of the resistor legs. The location and dimensions of the piezoresistors are shown in Fig. 2, and Table 1 summarizes other dimensions and material properties of the sensor.

The polysilicon diaphragms are formed by a surface micromachining process based on

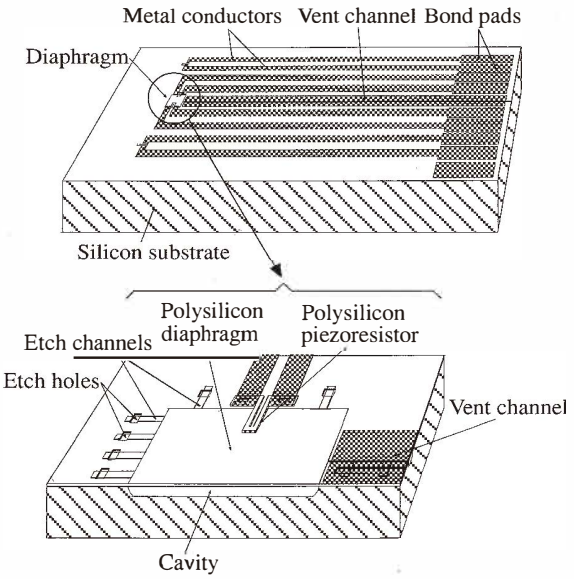

Fig. 1. Schematic of the sensor and a close-up of the diaphragm. The silicon chip size is $4 \times 2 \times 0.5$ mm and the diaphragm area is 100×100 μm.

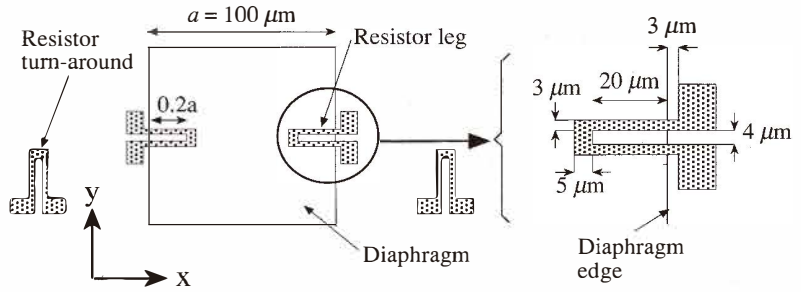

Fig. 2. Schematic top view of piezoresistor layout with the dimensions of the piezoresistors for a 100-μm-diaphragm microphone.

the formation of free-standing polysilicon diaphragms using sacrificial oxide-layer etching techniques in combination with etch channels to the vent channel and the diaphragm cavity. These etch channels are then sealed with a dielectric silicon nitride layer which is also used to insulate the piezoresistors on the diaphragms. Figure 3 shows a scanning electron microscopy (SEM) micrograph of the fabricated microphone.

Table 1
Dimensions and material properties of the sensor.

Diaphragm	side length, a	100 μm	
(polysilicon):	thickness, t_d	0.4 μm	
	Young's modulus, E	160 GPa	
	Poisson's ratio, μ	0.3	
	initial stress, ε_0	0.014%	ref. 9
	density, ρ_d	2300 kg/m^3	
Cavity:	depth, d	3 μm	
Vent channel:	length, l	3 mm	
	width, b	5 μm	
	height, h	0.1 μm	
Gas (air):	density, ρ_f	1.18 kg/m^3	
	kinematic viscosity, η	15.2×10^{-6} Pa/s	ref. 3
	compressibility, κ	7.14×10^{-6} m^2/N	ref. 3
Piezoresistors	thickness, t_g	0.3 μm	
(polysilicon)	electrical resistance, R	2.7 kΩ	
	parallel gauge factor, G_{par}	22.5	ref. 10
	perpend. gauge factor, G_{per}	–8.0	ref. 10

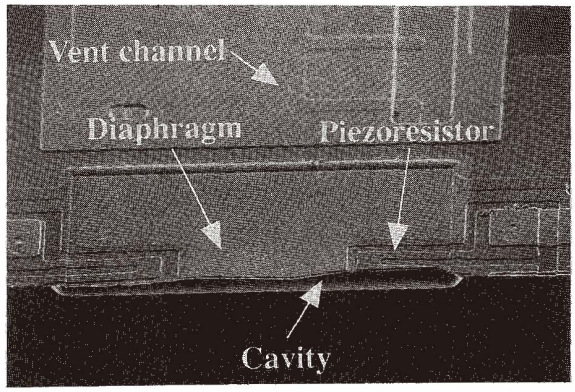

Fig. 3. A SEM micrograph of a cross section of the fabricated pressure sensor.

3. Theory

The important mechano-acoustical elements of the sensor are the diaphragm, the cavity, the added mass (due to the air in front of the diaphragm) and the vent channel. The latter is used to equalize the static air pressure difference between the cavity and the ambient. In the present design, the piezoresistors are located on the diaphragm, and it is assumed that these gauges have negligible mechanical influence on the mechano-acoustical behavior of the sensor since they are relatively small.

In this section, an energy method is described which is based on the different energy and power contributions of the sensor. However, the complexity of the obtained equation system forces us to use an electrical analogy method in which the equivalent electrical impedances are derived from the energy and power terms. In the first step of the analysis, the frequency response and the diaphragm center deflection amplitude, $z_0^{\max}$, of the microphone are derived. The second step involves the derivation of the pressure sensitivity of the microphone using the strain of the piezoresistors, which is transferred from the diaphragm stress distribution.

3.1 *Energy method*

To derive a method for accurate analytical calculations and to obtain a physical understanding of the acoustical behavior, the piezoresistive microphone is simulated using an energy method. In this method, the external pressure power, the potential and kinetic energy contributions and the power dissipation of the vent channel are calculated.

For a piezoresistive pressure sensor with a circular diaphragm, a clamped plate model can be used to describe the deflection shape of the diaphragm. For the calculation of the diaphragm center-deflection amplitude, $z_0^{\max}$, the tensile stresses must be included in the model.[11] To simplify the theoretical treatment a similar approach is used in this paper and the square diaphragm is assumed to be perfectly clamped. The deflection shape of the square diaphragm is approximated by

$$z(x,y,t) = z_0(t)\cdot\left(1-\left(\frac{2x}{a}\right)^2\right)^2\left(1-\left(\frac{2y}{a}\right)^2\right)^2\cdot \left[1+0.264\left(\left(\frac{2x}{a}\right)^2+\left(\frac{2y}{a}\right)^2\right)+0.309\left(\left(\frac{2x}{a}\right)^2\left(\frac{2y}{a}\right)^2\right)\right], \tag{1}$$

where a is the side length and $z_0(t)$ is the time-dependent center deflection of the diaphragm.[5] This relatively complex diaphragm shape is chosen since it can be used for very precise predictions of the resonance frequency and the maximum bending strain for a clamped square plate without built-in stress. A comparison between three different diaphragm deflection shapes, commonly reported in the literature, is given in the appendix.

A pressure $p_d(t) = p_d^{\max}\sin(\omega t)$ acting on the diaphragm results in a center-deflection variation of $z_0(t) = z_0^{\max}\sin(\omega t + \alpha)$ with a corresponding volume variation due to the diaphragm deflection of $\Delta V_d(t) = Sz_0^{\max}\sin(\omega t + \alpha)$. Here, $S = a^2/3.25$ is defined as the effective area (see appendix) and α as the phase angle between the flow and the diaphragm deflection. Then the dynamic volume flow created by the oscillating diaphragm is

$$q_d(t) = Sz_0^{\max}\omega\cos(\omega t + \alpha). \tag{2}$$

This volume flow from the diaphragm is divided between the cavity, $q_c(t)$, where the fluid

is compressed, and the vent channel, $q_v(t)$. These two volume flows can be expressed as

$$q_c(t) = BSz_0^{max}\omega\cos(\omega t + \alpha + \beta) \tag{3a}$$

$$q_v(t) = CSz_0^{max}\omega\cos(\omega t + \alpha + \gamma), \tag{3b}$$

where the parameters B and C describe the amplitudes of the two volume flows and β and γ are the phase angles related to the main flow.

The energy and power terms of the sensor elements are calculated based on the diaphragm deflection shape model of eq. (1). These calculations, shown in the appendix, yield the energy and power contributions which are summarized in Table 2. The subscripts e, k, p and l refer to external, kinetic, potential and energy losses, respectively, and the superscripts pres, bend, tens, dia, front, cav and vent refer to energies associated with the external pressure, bending and tensile forces on the diaphragm, the diaphragm, the fluid in front of the diaphragm, the cavity and the vent channel, respectively.

To be able to calculate the six unknown parameters z_0^{max}, B, C, α, β and γ, the following three physical relations are used.

- Continuity of volume flow requires that the volume flow from the diaphragm be the same as the sum of the volume flow which is compressed in the cavity and the volume flow through the vent channel, i.e., $q_d(t) = q_c(t) + q_v(t)$. This leads to

$$\cos(\omega t + \alpha) = B\cos(\omega t + \alpha + \beta) + C\cos(\omega t + \alpha + \gamma). \tag{4}$$

- The general expression for the acoustic power $p(t)$ is defined as[12]

$$P(t) = p(t) \cdot q(t), \tag{5}$$

where $P(t)$ is the pressure and $q(t)$ the volume flow. The pressure due to the air compression in the cavity must be the same as the pressure over the vent channel. Using the power expressions from Table 2 and the volume flows defined by eq. (3) we obtain

$$\frac{B\kappa^{-1}}{da^2}\sin(\omega t + \alpha + \beta) = \frac{1.2C\omega l}{bh}\left(\frac{10\eta}{h^2}\cos(\omega t + \alpha + \gamma) - \omega\rho_f\sin(\omega t + \alpha + \gamma)\right). \tag{6}$$

- The power supplied by the fluctuating outside pressure equals the sum of kinetic and potential powers and friction losses, which can be expressed as

$$P_e^{pres} = P_p^{bend} + P_p^{tens} + P_p^{cav} + P_k^{front} + P_k^{vent} + P_l^{vent}. \tag{7}$$

Equations (4), (6) and (7) are used to obtain the six unknown parameters, where the center-deflection amplitude, z_0^{max}, is the most noteworthy. The solution of this complex

Table 2
The energy and power contributions of the sensor elements.

Energy [J]	Power [W]
	$P_e^{pres} = p_d S z_0^{max} \sin(\omega t)\cos(\omega t + \alpha)$
$W_p^{bend} = \frac{65.8 E t_d^3 S}{2(1-\mu^2)a^4}(z_0^{max})^2 \sin^2(\omega t + \alpha)$	$P_p^{bend} = \frac{65.8 E t_d^3 S}{(1-\mu^2)a^4}(z_0^{max})^2 \omega \sin(\omega t + \alpha)\cos(\omega t + \alpha)$
$W_p^{tens} = \frac{15.0 t_d E \varepsilon_0 S}{2(1-\mu)a^2}(z_0^{max})^2 \sin^2(\omega t + \alpha)$	$P_p^{tens} = \frac{15.0 t_d E \varepsilon_0 S}{(1-\mu)a2}(z_0^{max})^2 \omega \sin(\omega t + \alpha)\cos(\omega t + \alpha)$
$W_p^{cav} = \frac{\kappa^{-1} S^2}{2da^2} B^2 (z_0^{max})^2 \sin^2(\omega t + \alpha + \beta)$	$P_p^{cav} = \frac{\kappa^{-1} S^2}{da^2} B^2 (z_0^{max})^2 \omega \sin(\omega t + \alpha + \beta)\cos(\omega t + \alpha + \beta)$
$W_k^{dia} = \frac{\rho_d t_d a^2}{2 \cdot 5.48}(z_0^{max})^2 \omega^2 \cos^2(\omega t + \alpha)$	$P_k^{dia} = -\frac{\rho_d t_d a^2}{5.48}(z_0^{max})^2 \omega^3 \sin(\omega t + \alpha)\cos(\omega t + \alpha)$
$W_k^{front} = \frac{\rho_f a^3}{2 \cdot 21.1}(z_0^{max})^2 \omega^2 \cos^2(\omega t + \alpha)$	$P_k^{front} = -\frac{\rho_f a^3}{21.1}(z_0^{max})^2 \omega^3 \sin(\omega t + \alpha)\cos(\omega t + \alpha)$
$W_k^{vent} = \frac{1.2 \rho_f l S^2}{2bh} C^2 (z_0^{max})^2 \omega^2 \cos^2(\omega t + \alpha + \gamma)$	$P_k^{vent} = -\frac{1.2 \rho_f l S^2}{bh} C^2 (z_0^{max})^2 \omega^3 \sin(\omega t + \alpha + \gamma)\cos(\omega t + \alpha + \gamma)$
$W_l^{vent} = \frac{12 \eta l \pi S^2}{bh^3} C^2 (z_0^{max})^2 \omega$ [a]	$P_l^{vent} = \frac{12 \eta l S^2}{bh^3} C^2 (z_0^{max})^2 \omega^2 \cos^2(\omega t + \alpha + \gamma)$

[a] Average energy during one period.

equation system is very laborious and therefore not recommended. However, a physical understanding is obtained which is a good foundation for the electrical analogy described below.

3.2 *Electrical analogy method*

An electrical analogy can be employed for theoretical characterization of the microphone.[4] With this approach, the physical system is described by mechano-acoustical characteristic parameters which are used as equivalent electrical impedances. A simplified equivalent circuit of the piezoresistive microphone is shown in Fig. 4. In this model, the pressure, p [N/m^2], is equivalent to voltage, the volume velocity, q [m^3/s], to current and the acoustic mass, M_a [kg/m^4], to inductance. The damping due to the viscosity of the gas is described by resistance R_a [Ns/m^5], and the capacitance, C_a [m^5/N], describes the diaphragm stiffness due to bending and tensile forces and gas compressibility. The external pressure at the diaphragm is represented by a voltage source, p_d. The equivalent electrical impedances can be derived using the following definitions of potential energy, kinetic energy and average acoustic power,[4]

$$W_p = \frac{(\Delta V)^2}{2C_a} \tag{8a}$$

$$W_k = \frac{M_a q^2}{2} \tag{8b}$$

$$P_l = R_a \tilde{q}^2, \tag{8c}$$

where ΔV is the volume variation due to diaphragm deflection, q the volume flow and $\tilde{q}$ the average volume flow. Using the energy and power expressions in Table 2 the equivalent electrical impedances are derived, and are shown in Table 3.

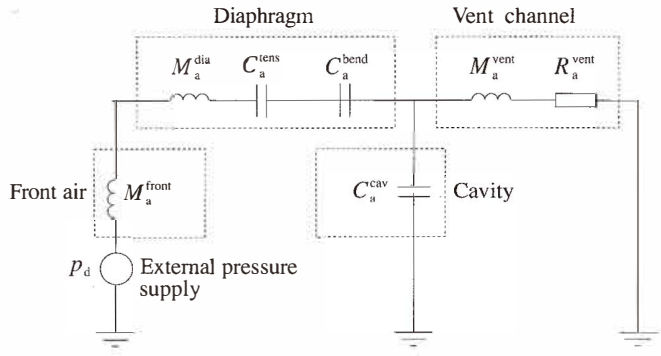

Fig. 4. An electrical analogy describing the equivalent acoustical circuit of the pressure transducer.

Table 3
The characteristic equivalent electrical impedances of the piezoresistive 100 μm diaphragm microphone.

Diaphragm	
– acoustical compliance (bending force)	$C_a^{bend} = \frac{(1-\mu^2)a^4 S}{65.8 E t_d^3}$ [m^5/N]
– acoustical compliance (tensile force)	$C_a^{tens} = \frac{(1-\mu^2)a^2 S}{15.0 E \varepsilon_0 t_d}$ [m^5/N]
– acoustical mass	$M_a^{dia} = \frac{\rho t_d a^2}{5.48 S^2}$ [kg/m^4]
Front air	
– acoustical mass	$M_a^{front} = \frac{\rho_f a^3}{21.1 S^2}$ [kg/m^4]
Cavity	
– acoustical compliance	$C_a^{cav} = \frac{d a^2}{\kappa^{-1}}$ [m^5/N]
Vent channel	
– acoustical resistance	$R_a^{vent} = \frac{12 \eta l}{b h^3}$ [Ns/m^5]
– acoustical mass	$M_a^{vent} = \frac{1.2 \rho_f l}{b h}$ [kg/m^4]

By using this method, which requires an analytical expression of the diaphragm deflection shape, the energy contributions of the mechanical and acoustical elements are first evaluated with an analytical energy method and then identified as equivalent electrical impedances. In this manner, two very major limitations of the conventional equivalent electrical circuit method are prevented.[7] Firstly, by using this method, analytical expressions for the equivalent electrical impedances can be derived for more complex mechanical and acoustical structures than the ones which are reported in the literature. Secondly, the conventional electrical analogy is restricted by the assumption of a one-dimensional displacement condition which means that a diaphragm is treated as being flat with pistonlike behavior. While the deflection shape can be used for analytical derivation of the stress of the diaphragm (see section 3.4 below), this would make it impossible to evaluate the strain of the gauges.

3.3 *Frequency response*

The equivalent electrical circuit of Fig. 4 can be easily analyzed using, *e.g.*, the $j\omega$ method. The center deflection, z_0^{max}, which is used for the pressure frequency response, is calculated by identifying the volume flow (the current) of the circuit with $q_d(t) = S z_0^{max} \omega \cos(\omega t + \alpha)$, yielding[12]

$$z_0^{\max} = \frac{p_d^{\max} / S}{\left[\frac{1}{C_a^{\text{bend}}} + \frac{1}{C_a^{\text{tens}}} - \omega^2 \left(M_a^{\text{dia}} + M_a^{\text{front}}\right) + \frac{j\omega\left(R_a^{\text{vent}} + j\omega M_a^{\text{vent}}\right)}{\left(\left(R_a^{\text{vent}} + j\omega M_a^{\text{vent}}\right) j\omega C_a^{\text{cav}} + 1\right)}\right]}. \quad (9)$$

Figure 5 shows the frequency response curve calculated from eq. (9). For low frequencies, the volume flow goes mainly through the vent channel. For higher frequencies there is no flow through the vent channel and all air volume associated with the diaphragm deflection is compressed in the cavity. The upper frequency limit is the resonance frequency.

This sensor is designed to operate in the mode where all of the gas flow is compressed in the cavity and there is no vent channel flow. This means that the theoretical center-deflection amplitude of the diaphragm in this flat part of the frequency response, derived from eq. (9), is

$$z_0^{\max} = \frac{p_d^{\max}}{\left(\frac{65.8 E t_d^3}{(1-\mu^2)a^4} + \frac{15.0 t_d E \varepsilon_0}{(1-\mu)a^2} + \frac{0.308 \kappa^{-1}}{d}\right)}. \quad (10)$$

The advantage of the design with a long and narrow vent channel is that the vent channel outlet can be exposed to the outside pressure fluctuations without affecting the diaphragm deflection. The lower limiting cut-off frequency, f_c, is defined as the frequency

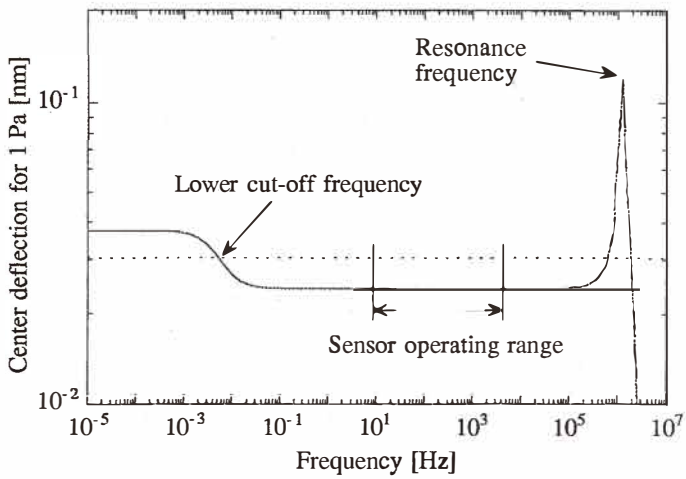

Fig. 5. Theoretical frequency response of the 100-μm-diaphragm microphone. The curve shows that the sensor has a theoretical frequency operation range of 2 mHz $< f <$ 1.4 MHz which suffiently covers the measured turbulence frequency range of 10 Hz $< f <$ 25 kHz.

when the sensitivity is the average of the sensitivity level dominated by compressible cavity flow and that dominated by vent channel flow. Calculated from eq. (9), this yields

$$f_c = \frac{1}{\left(\frac{(1-\mu^2)a^4}{65.8Et_d^3} + \frac{(1-\mu)a^2}{15.0E\varepsilon_0 t_d} + \frac{d}{0.308\kappa^{-1}} \right) \frac{24\pi\eta lS}{bh^3}}. \tag{11}$$

For the 100 μm sensor this lower limiting frequency is 2 mHz which is well below the lowest frequency of interest of about 10 Hz for turbulent measurement applications. For higher frequencies the theoretical frequency response is flat until it reaches the resonance frequency. For the calculation of the resonance frequency the flow through the vent channel can be neglected. Using eq. (9), the fundamental transversal bending-mode resonance frequency of the diaphragm is

$$f_0 = \frac{1}{2\pi} \sqrt{\frac{\left(\frac{65.8Et_d^3 S}{(1-\mu^2)a^4} + \frac{15.0t_d E\varepsilon_0 S}{(1-\mu)a^2} + \frac{\kappa^{-1}S^2}{da^2} \right)}{\left(\frac{\rho_d t_d a^2}{5.48} + \frac{\rho_f a^3}{21.1} \right)}}. \tag{12}$$

For the 100 μm sensor, this resonance frequency is 1.4 MHz. Since the highest frequency of interest for turbulent measurements is about 25 kHz the sensor has no resonance peaks in the range in which the measurements are made. It is concluded that the sensor has a very broad theoretical frequency response, much wider than the frequency range required for turbulence measurements, as can be seen in Fig. 5.

It is interesting to note that the information on the diaphragm center deflection, cut-off and resonance frequencies can all be derived from the same expression, eq. (9), which is possible due to a combination of the extended energy and electrical analogy methods.

3.4 *Pressure sensitivity*

The resistor configuration of this microphone, shown in Fig. 3, has two active piezoresistors positioned on the diaphragm and two passive resistors positioned beside the diaphragm. With a diaphragm thickness of t_d and a resistor thickness of t_g the average distance between an active piezoresistor and the middle of the diaphragm is $(t_d + t_g)/2$. In the case where the diaphragm deflection is small compared with its thickness, the strains ε_x and ε_y acting on the strain gauges are[10]

$$\varepsilon_x = -\frac{(t_d + t_g)}{2} \left(\frac{\partial^2 z}{\partial x^2} + \mu \frac{\partial^2 z}{\partial y^2} \right) \tag{12a}$$

$$\varepsilon_y = -\frac{(t_d + t_g)}{2}\left(\frac{\partial^2 z}{\partial y^2} + \mu\frac{\partial^2 z}{\partial x^2}\right) \tag{12b}$$

The resistance changes of the legs (the straight parts) and the turn-around (the U-shaped parts) of the active strain gauges are

$$\left(\frac{\Delta R}{R}\right)_x = G_{par} < \varepsilon_x > + G_{per} < \varepsilon_y > \tag{13a}$$

$$\left(\frac{\Delta R}{R}\right)_y = G_{per} < \varepsilon_x > + G_{par} < \varepsilon_y >, \tag{13b}$$

respectively, where G_{par} and G_{per} are the transverse and longitudinal gauge factors, respectively, and $<\varepsilon_x>$ and $<\varepsilon_y>$ the average strains in the x- and y-directions, respectively. For the 100-μm-diaphragm layout, with the dimensions and constants shown in Table 1 and Fig. 2, the total change of resistance of an active strain gauge is

$$\left(\frac{\Delta R}{R}\right)_{tot} = \frac{z_0 (t_d + t_g)}{2a^2}\left[(8.31G_{par} + 1.32G_{per}) + (-1.23G_{par} - 0.92G_{per})\right], \tag{14}$$

where, within the square brackets, the first parenthesized term originates from eq. (13a) and the second from eq. (13b). The pressure sensitivity S^p, defined as the relative change of output voltage per unit of applied differential pressure, for the sensor with two active and two passive piezoresistors connected in a Wheatstone bridge is then

$$S^p = \frac{\Delta V_{out}}{\Delta p_d V_b} = \frac{(1.77G_{par} + 0.1G_{per})(t_d + t_g)}{\left(\frac{65.8Et_d^3}{(1-\mu^2)a^2} + \frac{15.0E\varepsilon_{\bullet}t_d}{(1-\mu)} + \frac{0.308\bullet^2\kappa^{-1}}{d}\right)} \text{ [V/V/Pa]}, \tag{15}$$

where V_b is the bridge supply voltage. This equation describes the expected dynamical sensitivity for small pressure amplitudes in the chosen frequency range of operation for the sensor, i.e., for frequencies higher than the lower cut-off frequency defined by eq. (11), but for frequencies lower than the first resonance frequency defined by eq. (12). Using the material and design parameters of Table 1, the acoustical pressure sensitivity for the 100 μm sensor is 0.75 μV/Pa for a bridge supply voltage of 10 V. The static diaphragm sensitivity, i.e., the pressure sensitivity of the sensor for low frequencies, is controlled by the vent channel flow and is 1.2 μV/Pa according to eq. (15), but without the third term in the denominator. All calculated characteristics of the sensor are shown in Table 4.

Table 4
Calculated and measured characteristics of the fabricated microphone.

Theory		
Lower cut-off frequency	:	2 mHz
Resonance frequency	:	1.4 MHz
Acoustical sensitivity at 10 V	:	0.75 μV/Pa
Static diaphragm sensitivity at 10 V	:	1.2 μV/Pa
Measurements		
Frequency bandwidth	:	10 Hz~10 kHz (±2 dB)
Acoustical sensitivity at 10 V	:	0.9 μV/Pa
Static diaphragm sensitivity at 10 V	:	1.2 μV/Pa[a]
Noise (A-weighted)	:	96 dB(A)

[a]Derived from large-deflection diaphragm measurements.

4. Experimental Results and Discussion

The frequency characteristics of the microphone were measured using a Brüel & Kjaer Type 4226 closed coupler with a built-in reference microphone at a sound pressure level of 114 dB. The measurements were performed for a bridge supply voltage of 10 V and show an acoustical sensitivity of about 0.9 μV/Pa for a diaphragm side length of 100 μm. The small deviations from the theoretical estimations for the acoustical sensitivity of 0.75 μV/Pa can be attributed to the approximations in the sensitivity calculation and to the uncertainty in the magnitudes of the built-in stresses in the polysilicon diaphragm. The static sensitivity was measured taking into account that the cavity was vacuum sealed during its fabrication. By comparing the resistance of the strain gauges before and after opening the vent channel, the static sensitivity could easily be deduced. It should be noted that for the relatively high pressure of 10^5 Pa, the diaphragm behaves nonlinearly, and the measured static sensitivity should not be directly compared to the calculated values. A typical measured frequency response is shown in Fig. 6. The curve shows good flatness within ± 2 dB in the range of 10 Hz to 10 kHz. The deviations for high frequencies originate from interference in the coupler and are not characteristics of the microphone. An indication which supports this conclusion is that a larger, similarly fabricated transducer with a 300 μm diaphragm reveals the same deviations. The noise of the microphones has $1/\sqrt{f}$ dependence and an acoustic noise level of 96 dB(A) for a microphone having a sensitivity of 0.9 μV/Pa. The measured characteristics of the silicon microphone are summarized in Table 4.

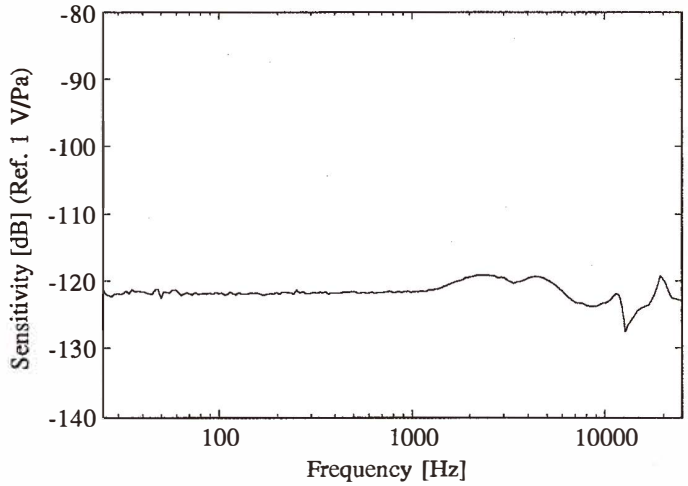

Fig. 6. Measured frequency response of a sensor with a 100 μm diaphragm for a bridge supply voltage of 10 V.

5. Conclusions

An energy method has been used for the theoretical derivation of the characteristics of a square-diaphragm piezoresistive microphone. The center-deflection frequency response as well as the pressure sensitivity of the microphone has been calculated. For simplification, the energy and power expressions have been described as equivalent electrical impedances and an electrical analogy has been employed. All relevant energy terms are included, corresponding to the stiffness of the diaphragm to bending and tensile forces, the acoustical mass of the diaphragm and of the fluid in front of the diaphragm, the stiffness of the air-gap cavity and the acoustical mass, as well as the frictional losses of the vent channel. It has been concluded that this method is very useful for the calculation of the characteristics of an acoustic sensor. It can be used to derive the characteristics of much more complex mechano-acoustical structures than the microphone demonstrated here. The results of the analysis have been compared with experimental data from fabricated microphones, and have shown good agreement.

Acknowledgment

This work was supported by the Swedish Research Council for Engineering Sciences (TFR).

Appendix

This appendix is divided into two sections, A and B. In section A the energy and power expressions for the microphone elements are derived. In section B the dependences on the resonance frequency and the maximum strain for different diaphragm deflection shapes are described.

A. Calculation of energy and power expressions

Using the energy method, the frequency response as well as the center deflection of the diaphragm can be derived by taking all relevant energy contributions into account. Here in the appendix, these energy terms, that is, the stiffness of the diaphragm to bending and tensile forces, the acoustical mass of the diaphragm and the air in the front of the diaphragm, the stiffness of the air-gap cavity, and the acoustical mass as well as the frictional losses of the vent channel, are calculated.

The time-dependent diaphragm deflection shape can be described by[5]

$$z(x,y,t) = z_0(t)\cdot g(x,y) = z_0(t)\cdot\left(1-\left(\frac{2x}{a}\right)^2\right)^2\left(1-\left(\frac{2y}{a}\right)^2\right)^2 \cdot \left[1+0.264\left(\left(\frac{2x}{a}\right)^2+\left(\frac{2y}{a}\right)^2\right)+0.309\left(\left(\frac{2x}{a}\right)^2\left(\frac{2y}{a}\right)^2\right)\right] \quad [\mathrm{m}], \tag{A1}$$

where a is the side length, $z_0(t) = z(x = 0, y = 0, t)$ is the center deflection and $g(x, y)$ describes the deflection shape of the diaphragm. For the dynamic derivations, the pressure on the diaphragm is assumed to have a time dependence of $p_a(t) = p_d^{\max}\sin(\omega t)$. With α as the phase angle between the supplied pressure and the diaphragm deflection, the diaphragm center deflection is $z_0(t) = z_0^{\max}\sin(\omega t + \alpha)$. This leads to a diaphragm velocity in the z-direction of $v(x,y,t) = z_0^{\max} g(x,y)\omega\cos(\omega t + \alpha)$. The diaphragm volume deflection and flow from the diaphragm are then

$$\Delta V_d(t) = S z_0^{\max}\sin(\omega t + \alpha) \quad [\mathrm{m}^3] \tag{A2}$$

$$q_d(t) = S z_0^{\max}\omega\cos(\omega t + \alpha) \quad [\mathrm{m}^3/\mathrm{s}], \tag{A3}$$

where the parameter S, the shape factor, is dependent on the deflection shape of the diaphragm and is given by

$$S = \int_{-a/2}^{a/2}\int_{-a/2}^{a/2} g(x,y)\,\mathrm{d}x\mathrm{d}y = \frac{a^2}{3.25} \quad [\mathrm{m}^2]. \tag{A4}$$

As can be seen in Fig. A1, the volume flow from the diaphragm is divided between the cavity, $q_c(t)$, where the volume is compressed, and the vent channel, $q_v(t)$. Due to volume

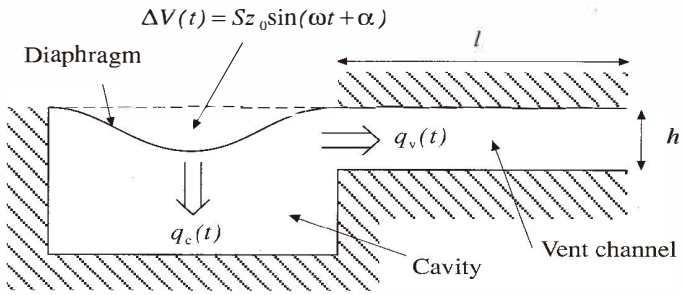

Fig. A1. Schematic model of a cross section of the microphone.

flow continuity one obtains $q_d(t) = q_c(t) + q_v(t)$. These two volume flows can be expressed as

$$q_c(t) = BSz_0^{max}\omega\cos(\omega t + \alpha + \beta) \ [m^3/s] \tag{A5a}$$

$$q_v(t) = CSz_0^{max}\omega\cos(\omega t + \alpha + \gamma) \ [m^3/s], \tag{A5b}$$

where the parameters B and C describe the amplitudes of the two volume flows and β and γ are the phase angles related to the main flow.

The load deflection relationship of a square diaphragm has been derived using an energy minimization approach as[10,13]

$$p_d = \frac{65.8Et^3z_0}{a^4(1-\mu^2)} + \frac{15.0tE\varepsilon_0 z_0}{a^2(1-\mu)} + \frac{25.3Etz_0^3}{a^4(1-\mu^2)} \ [Pa]. \tag{A6}$$

Here, the first term corresponds to the bending forces, the second term to the built-in stresses of the diaphragm and the third term to stretching forces. For small deflections, stretching of the diaphragm can be neglected. Using these assumptions the energy and power terms are calculated below.

External pressure power

By using the expression for the acoustic power defined by eq. (5), the power of an oscillating external pressure $p_d(t) = p_d^{max}\sin(\omega t)$ acting on the diaphragm with a volume flow $q_d(t) = Sz_0^{max}\sin(\omega t + \alpha)$ is

$$P_e^{pres} = p_d(t) \cdot q_d(t) = p_d^{max}Sz_0^{max}\omega\sin(\omega t)\cos(\omega t + \alpha) \ [W]. \tag{A7}$$

Potential energy of the diaphragm due to bending forces

By using the diaphragm shape eq. (A1) and the first term of the center-deflection eq. (A6), the pressure $p_d(z)$ can be expressed as

$$p_d(z) = \frac{65.8Et_d^3}{(1-\mu^2)a^4} \cdot \frac{z}{g(x,y)} \text{ [Pa].} \tag{A8}$$

From this, the potential energy of the bending forces for a diaphragm with a certain center-deflection amplitude z_0^{max} is derived as

$$W_p^{bend} = \int_{-a/2}^{a/2} dx \int_{-a/2}^{a/2} dy \int_0^{z(x,y,t)} p_d(z)dz = \frac{65.8Et_d^3S}{2(1-\mu^2)a^4}(z_0^{max})^2 \sin^2(\omega t + \alpha) \text{ [J].} \tag{A9}$$

The change of energy per unit time, i.e., the power of this potential energy is calculated as

$$P_p^{bend} = \frac{\partial}{\partial t} W_p^{bend} = \frac{65.8Et_d^3S}{(1-\mu^2)a^4}(z_0^{max})^2 \omega \sin(\omega t + \alpha)\cos(\omega t + \alpha) \text{ [W].} \tag{A10}$$

Potential energy of the diaphragm due to tensile forces

The potential energy and the power of the diaphragm due to tensile forces are derived from eq. (A1) and (A6) in the same manner as that for the bending forces. This yields the tensile potential energy and power of the diaphragm as

$$W_p^{tens} = \frac{15.0t_dE\varepsilon_0 S}{2a^2(1-\mu)}(z_0^{max})^2 \sin^2(\omega t + \alpha) \text{ [J]} \tag{A11}$$

$$P_p^{tens} = \frac{\partial}{\partial t} W_p^{tens} = \frac{15.0t_dE\varepsilon_0 S}{a^2(1-\mu)}(z_0^{max})^2 \omega \sin(\omega t + \alpha)\cos(\omega t + \alpha) \text{ [W].} \tag{A12}$$

Potential energy of the fluid in the cavity

A volume V of a compressible fluid with a volume variation ∂V is subjected to a pressure variation defined as[4]

$$\partial p = -\frac{\kappa^{-1}\partial V}{V} \text{ [Pa],} \tag{A13}$$

where κ is the compressibility of the fluid. The pressure in the cavity, $p_c(t)$, which arises

due to the diaphragm center deflection, is then calculated as

$$p_c(t) = \frac{\kappa^{-1}\Delta V_c(t)}{V} = \frac{\kappa^{-1}BS}{da^2} z_0^{\max} \sin(\omega t + \alpha + \beta) \text{ [Pa]}, \tag{A14}$$

where $\Delta V_c(t) = BSz_0^{\max}\sin(\omega t + \alpha + \beta)$ is derived using eq. (A5a). From this, the power and the potential energy of the compressed gas in the cavity can be obtained using eq. (5) as

$$P_p^{cav} = \frac{\kappa^{-1}S^2}{da^2} B^2 (z_0^{\max})^2 \omega \sin(\omega t + \alpha + \beta)\cos(\omega t + \alpha + \beta) \text{ [W]} \tag{A15}$$

$$W_p^{cav} = \int P_p^{cav} dt = \frac{\kappa^{-1}S^2}{2da^2} B^2 (z_0^{\max})^2 \sin^2(\omega t + \alpha + \beta) \text{ [J]}. \tag{A16}$$

Kinetic energy of the diaphragm

The kinetic energy of a small element at (x,y) of the diaphragm can be defined as

$$\Delta W_k^{dia}(x,y,t) = \frac{1}{2}\Delta m v(x,y,t)^2 \text{ [J]}, \tag{A17}$$

where $\Delta m = \rho_d t_d \Delta x \Delta y$ and $v(x,y,t) = z_0^{\max} g(x,y)\,\omega\cos(\omega t + \alpha)$. The total kinetic energy and power of the diaphragm are then

$$W_k^{dia} = \int_{-a/2}^{a/2}\int_{-a/2}^{a/2} \Delta W_k^{dia}(x,y,t)\,dx\,dy = \frac{\rho_d t_d \omega^2 a^2}{2 \cdot 5.48}(z_0^{\max})^2 \cos^2(\omega t + \alpha) \text{ [J]} \tag{A18}$$

$$P_k^{dia} = \frac{\partial}{\partial t} W_k^{dia} = -\frac{\rho_d t_d \omega^3 a^2}{5.48}(z_0^{\max})^2 \sin(\omega t + \alpha)\cos(\omega t + \alpha) \text{ [W]}. \tag{A19}$$

Kinetic energy of the fluid over the diaphragm

When a diaphragm vibrates in a fluid, the fluid near the diaphragm is set into motion and the diaphragm radiates sound energy. Analysis of this phenomenon is very complex due to the three-dimensional character of the equations describing the fluid motion.[14] The fluid energy is due to the movement of the fluid over the diaphragm. This effect is the same as adding an equivalent mass of the fluid to the plate. One proposal for determining the added mass of the fluid over a plate is[15]

$$m_{add} = \lambda \rho_f a^3 \text{ [kg]}, \tag{A20}$$

where a is the side length of the diaphragm, ρ_f is the density of the fluid and λ is defined as

$$\lambda = \frac{\left(\int_{-a/2}^{a/2} \int_{-a/2}^{a/2} g(x,y)\,dx dy \right)^2}{2a^2 \int_{-a/2}^{a/2} \int_{-a/2}^{a/2} g(x,y)^2\,dx dy}. \tag{A21}$$

For the diaphragm deflection shape described by eq. (A1), λ is 0.26. Using this approximation, the kinetic energy and power of the fluid are calculated by replacing the diaphragm mass, $m = \rho_d t_d a^2$, of eq. (A17) with this added mass $m_{add} = \lambda \rho_f a^3$, yielding

$$W_k^{front} = 0.26 \frac{\rho_f a}{\rho_d t_d} W_k^{dia} = \frac{\rho_f \omega^2 a^3}{2 \cdot 21.1} (z_0^{max})^2 \cos^2(\omega t + \alpha) \ \text{[J]} \tag{A22}$$

$$P_k^{front} = \frac{\partial}{\partial t} W_k^{front} = -\frac{\rho_f \omega^3 a^3}{21.1} (z_0^{max})^2 \sin(\omega t + \alpha)\cos(\omega t + \alpha) \ \text{[W]}. \tag{A23}$$

Kinetic energy of the fluid in the vent channel

Poiseuille's parabolic law yields a velocity distribution in the vent channel, shown in Fig. A2, given by

$$v(z) = v_0 \left(1 - \left(\frac{2z}{h} \right)^2 \right) \ \text{[m/s]}. \tag{A24}$$

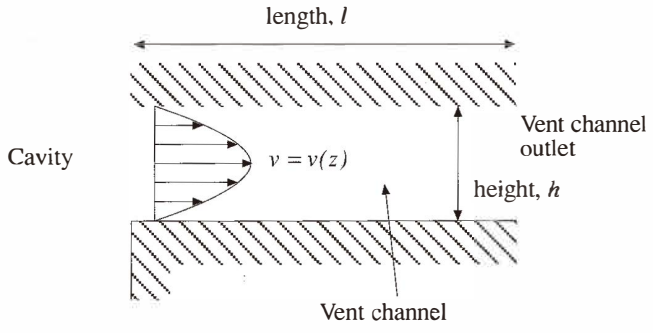

Fig. A2. Schematic cross section of the vent channel.

The volume flow through the slit is then

$$q_v = b \int_{-h/2}^{h/2} v(z)\mathrm{d}z = \frac{2bhv_0}{3} \quad [\mathrm{m^3/s}] \tag{A25}$$

assuming that the velocity is uniform over the width b. The kinetic energy of the fluid in the channel is then calculated by an integration over a slice Δz, moving at a velocity $v(z)$

$$\Delta W_k^{vent} = 0.5\rho_f blv^2(z)\Delta z \quad [\mathrm{J}]. \tag{A26}$$

By using the vent channel volume flow equation (A3b), the kinetic energy and power of the vent fluid are calculated as

$$W_k^{vent} = \int_{-h/2}^{h/2} \Delta W_k^{vent}\mathrm{d}z = \frac{4\rho_f lbhv_0^2}{15} = \frac{3\rho_f lS^2}{5bh} C^2 (z_0^{max})^2 \omega^2 \cos^2(\omega t + \alpha + \gamma) \quad [\mathrm{J}] \tag{A27}$$

$$P_k^{vent} = \frac{\partial}{\partial t} W_k^{vent} = -\frac{6\rho_f lS^2}{5bh} C^2 (z_0^{max})^2 \omega^3 \sin(\omega t + \alpha + \gamma)\cos(\omega t + \alpha + \gamma) [\mathrm{W}]. \tag{A28}$$

Frictional losses of the fluid in the vent channel

There is an energy loss in the channel caused by the friction forces which yield a pressure drop in the channel of[16]

$$p_v(t) = \frac{12\eta l}{bh^3} q_v(t) \quad [\mathrm{Pa}]. \tag{A29}$$

Since the channel is open, the flow velocity can be considered to be the same through the entire channel. According to eq. (5) this gives a power loss of

$$P_l^{vent} = p_v(t) \cdot q_v(t) = \frac{12\eta l}{bh^3} C^2 S^2 (z_0^{max})^2 \omega^2 \cos^2(\omega t + \alpha + \gamma) \quad [\mathrm{W}]. \tag{A30}$$

Integration of this equation gives the losses during one period as

$$W_l^{vent} = \int_0^T P_l^{vent}\mathrm{d}t = \frac{12\eta l\pi S^2}{bh^3} C^2 (z_0^{max})^2 \omega \quad [\mathrm{J}]. \tag{A31}$$

B. Resonance frequency and maximum strain for a clamped square plate

For an investigation of the diaphragm deflection shape model which has been used in this paper, expressions for the resonance frequency as well as for the maximum strain of a square clamped plate with no built-in stresses are derived for three different deflection shapes.

The deflection of a diaphragm at a point (x,y) can be described as $z(x,y) = z_0 \cdot g(x,y)$, where z_0 is the center deflection and $g(x,y)$ describes the deflection shape of the diaphragm. The shape factor S and the effective mass m^* of the diaphragm are defined as

$$S = \int_{-a/2}^{a/2} \int_{-a/2}^{a/2} g(x,y)\mathrm{d}x\mathrm{d}y \quad [\mathrm{m}^2] \tag{A32}$$

$$m^* = \rho_\mathrm{d} t_\mathrm{d} \int_{-a/2}^{a/2} \int_{-a/2}^{a/2} g(x,y)^2 \mathrm{d}x\mathrm{d}y \quad [\mathrm{kg}], \tag{A33}$$

where ρ_d is the diaphragm density and t_d the diaphragm thickness.

By using the electrical analogy method described in this paper, the pressure affecting a clamped square plate, i.e., a diaphragm with dominating bending forces, can be described as a series resonance circuit with a voltage source (external pressure), an equivalent electrical inductance (acoustical mass) and a capacitor (bending stiffness). The acoustical mass is derived using eq. (8b) and (A18) as

$$M_\mathrm{a}^\mathrm{dia} = \frac{m^*}{S^2} \quad [\mathrm{kg/m^4}], \tag{A34}$$

and the bending stiffness capacitance using eq. (8a) and (A9) as

$$C_\mathrm{a}^\mathrm{bend} = \frac{(1-\mu^2)a^4 S}{65.8 E t_\mathrm{d}^3} \quad [\mathrm{m^5/N}]. \tag{A35}$$

The resonance frequency is then derived using the definition for a series resonance circuit as

$$f_0 = \frac{1}{2\pi\sqrt{C_\mathrm{a}^\mathrm{bend} M_\mathrm{a}^\mathrm{dia}}} = c_1 \frac{t_\mathrm{d}}{a^2}\sqrt{\frac{E}{\rho_\mathrm{d}(1-\mu^2)}} \quad [\mathrm{Hz}], \tag{A36}$$

where the numerical constant c_1 can be identified for different deflection shapes of the diaphragm.

The maximum strain of the top of a square plate which occurs at the center of the diaphragm edge is derived in analogy with the calculations in this paper in section 3.4 using eqs. (A6) and (12a). The resulting expression is

$$\varepsilon_x = c_2 \frac{a^2(1-\mu^2)p_d}{Et_d^2}, \tag{A37}$$

where the numerical constant c_2 can be identified for different deflection shapes in the same manner as that for the resonance frequency. For the third deflection shape with the circular diaphragm approximation and an equivalent radius of $a/\sqrt{\pi}$, the maximum strain is directed toward the center of the diaphragm.[11]

The results of these calculations including the shape factor S, the effective mass m^* and the two constants c_1 and c_2, are shown in Table A1 for three different diaphragm shapes. Comparing these constants with "accepted" values from the literature, it is found that the first deflection shape gives the best agreement.[10,14] This is the reason why this relatively complex expression has been chosen to describe the diaphragm deflection in this paper.

References

1 E. Kälvesten, L. Löfdahl and G. Stemme: Sensors and Actuators **A 45** (1994) 103.
2 E. Kälvesten, L. Löfdahl and G. Stemme: Sensors and Actuators **A 46** (1995) 151.
3 L. Löfdahl, E. Kälvesten and G. Stemme: Experiments in Fluids **17** (1994) 24.
4 M. Rossi: Acoustics and Electroacoustics (Artech House, Norwood, 1988) Chaps. 5 and 8.
5 S. Timoshenko and S. Woinowsky-Krieger: Theory of Plates and Shells (McGraw-Hill, New York, 1959) p. 202.
6 T. Bourouina, S. Spirkovitch, F. Baillieu and C. Vauge: Sensors and Actuators **A 31** (1992) 149.
7 J. Bergqvist: Sensors and Actuators **A 39** (1993) 191.
8 E. Stemme and G. Stemme: Sensors and Actuators **A 32** (1992) 639.
9 H. Guckel: Proc. 4th Int. Conf. Solid-State Sensors and Actuators (Transducers '87), Tokyo, 1987, p. 277.
10 H. Guckel: Sensors and Actuators **A 28** (1991) 133.
11 O. Tabata, K. Shimaoka, S. Sugiyama and I. Igarashi: Technical Digest of the 8th Sensor Symposium, Japan, 1989, p. 149.
12 L. Beranek: Acoustics (McGraw-Hill, New York, Toronto, London 1954) p. 61.
13 Z. Djuric, M. Matic, J. Matovic, R. Petrovic and N. Simicic: Sensors and Actuators **A 24** (1990) 175.
14 R. D. Blevins: Formulas for Natural Frequency and Mode Shape (Van Nostrand Reinold Company, New York, 1979) pp. 260 and 413.
15 J. E. Greespon: J. Acoustic. Soc. Am. **33** (1961) 1485.
16 G. Landsberg: Hütte: Des Ingenieurs Taschenbuch, Theoretische Grundlagen, (Ernst und Sohn, Berlin, 1955) p. 779.

Table A1
Some calculated parameters for different diaphragm shapes.

Diaphragm deflection-shape, $g(x,y)$ and $g(r)$	S	m^*	c_1	c_2
$\left(1-\left(\frac{2x}{a}\right)^2\right)^2\left(1-\left(\frac{2y}{a}\right)^2\right)^2$ $\left[1+0.264\left(\left(\frac{2x}{a}\right)^2+\left(\frac{2y}{a}\right)^2\right)+0.309\left(\left(\frac{2x}{a}\right)^2\left(\frac{2y}{a}\right)^2\right)\right]$	$\frac{a^2}{3.25}$	$\frac{\rho t a^2}{5.48}$	1.67	0.308
$\left(1-\left(\frac{2x}{a}\right)^2\right)^2\left(1-\left(\frac{2y}{a}\right)^2\right)^2$	$\frac{a^2}{3.52}$	$\frac{\rho t a^2}{6.05}$	1.69	0.243
$\left(1-\left(\frac{r}{a}\right)^2\right)^2$ (equivalent radius $\frac{a}{\sqrt{\pi}}$)	$\frac{a^2}{3}$	$\frac{\rho t a^2}{5}$	1.48	0.239
Refs. 10 and 14			1.65	0.308

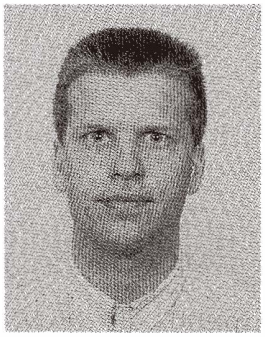

Edvard Kälvesten was born in Uppsala, Sweden, on November 11, 1967. He received his M.Sc. degree in Physical Engineering in 1992 from Chalmers University of Technology, Göteborg, Sweden. At present, he is a graduate student in the Silicon Sensor Research Group at the Department of Signals, Sensors and Systems at the Royal Institute of Technology, Stockholm, Sweden. His work concerns micromachined silicon sensors, especially for turbulence applications.

Lennart Löfdahl was born in Trollhättan, Sweden, on June 21, 1948. He received both his M.Sc. degree in Mechanical Engineering in 1975 and Ph.D. in Thermo- and Fluid Dynamics in 1982, from Chalmers University of Technology (CTH), Göteborg, Sweden. He was researcher at the Swedish Maritime Research Institute (SSPA) from 1981 to 1984. In 1984, Dr. Löfdahl rejoined the Department of Thermo- and Fluid Dynamics at CTH where he became an Associate Professor in 1987, heading a turbulence research group. His research is devoted to experimental fluid dynamics with special emphasis on turbulence measurements and modelling incompressible flows.

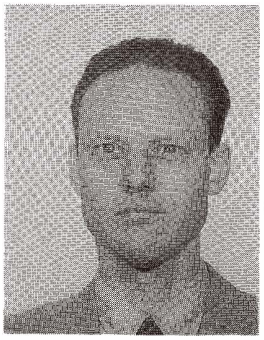

Göran Stemme was born in Stockholm, Sweden, on February 4, 1958. He received both his M.Sc. degree in electrical engineering in 1981 and the Ph.D. in Solid State Electronics in 1987, from Chalmers University of Technology, Göteborg, Sweden. In 1981, he joined the Department of Solid State Electronics at Chalmers University of Technology and in 1990, he became an Associate Professor heading the Silicon Sensor Research Group. In 1991, Dr. Stemme was appointed Professor at the Royal Institute of Technology, Stockholm, Sweden. He heads research on sensors and actuators based on micromachining of silicon at the Department of Signals, Sensors and Systems.